Dynamics of Isolated Convective Regions in the Ocean

MARTIN VISBECK, JOHN MARSHALL, AND HELEN JONES

Center for Meteorology and Physical Oceanography, Department of Earth, Atmospheric and Planetary Science, Massachusetts Institute of Technology, Cambridge, Massachusetts

(Manuscript received 6 December 1994, in final form 20 October 1995)

ABSTRACT

An initially resting ocean of stratification N is considered, subject to buoyancy loss at its surface of magnitude B_0 over a circular region of radius r, at a latitude where the Coriolis parameter is f. Initially the buoyancy loss gives rise to upright convection as an ensemble of plumes penetrates the stratified ocean creating a vertically mixed layer. However, as deepening proceeds, horizontal density gradients at the edge of the forcing region support a geostrophic rim current, which develops growing meanders through baroclinic instability. Eventually finite-amplitude baroclinic eddies sweep stratified water into the convective region at the surface and transport convected water outward and away below, setting up a steady state in which lateral buoyancy flux offsets buoyancy loss at the surface. In this final state quasi-horizontal baroclinic eddy transfer dominates upright "plume" convection.

By using "parcel theory" to consider the energy transformations taking place, it is shown that the depth, h_{final}, at which deepening by convective plumes is arrested by lateral buoyancy flux due to baroclinic eddies, and the time t_{final} it takes to reach this depth, is given by

$$h_{\text{final}} = \gamma \frac{(B_0 r)^{1/3}}{N}, \quad t_{\text{final}} = \beta \left(\frac{r^2}{B_0} \right)^{1/3},$$

both independent of rotation. Here γ and β are dimensionless constants that depend on the efficiency of baroclinic eddy transfer. A number of laboratory and numerical experiments are then inspected and carried out to seek confirmation of these parameter dependencies and obtain quantitative estimates of the constants. It is found that $\gamma = 3.9 \pm 0.9$ and $\beta = 12 \pm 3$.

Finally, the implications of our study to the understanding of integral properties of deep and intermediate convection in the ocean are discussed.

1. Introduction

Deep and intermediate water masses of the world's oceans are thought to form in localized regions of subpolar gyres. The convective overturning of the water column occurs through the agency of many intense plumes, which vigorously mix the column. Working in concert, the plumes can process vast volumes of fluid to form what has become known as a "chimney" of homogenized fluid. The "plume scale" is ~1 km; that of the chimney some, perhaps many, tens of kilometers.

In recent years there has been much interest in the dynamics of plumes—they have been the focus of observational, laboratory, numerical, and theoretical study. The advent of modern technologies such as the moored acoustic Doppler current profiler (ADCPs) revealed strong vertical velocities during intense cooling periods in late winter associated with deep convection (Schott and Leaman 1991; Schott et al. 1993). It was those time series that enabled estimates to be made of the intensity and scale of the "plumes" (Visbeck 1993; Schott et al. 1994). Motivated by such observations, laboratory and numerical experiments (Maxworthy and Narimousa 1994; Jones and Marshall 1993) led to physically motivated scaling laws for key aspects of the plumes.

More recently, Send and Marshall (1995) turned their attention to the chimney scale and considered the integral effect of many such plumes. They argued that rather than acting as conduits that carry significant volumes of fluid from the surface to great depth, plumes are best thought of as efficient mixing agents, responsible solely for "churning" the column. They placed emphasis on the role of geostrophic eddies that develop in the baroclinic zone on the periphery of the chimney, controlling exchange of fluid between the chimney and its surroundings. Such baroclinic eddies have been observed in the ocean along the edge of a convective chimney in the Mediterranean Sea (Gascard 1978) and in the Labrador Sea (Gascard and Clarke 1983). Theo-

Corresponding author address: Dr. Martin Visbeck, Physical Oceanography, Lamont-Doherty Earth Observatory of Columbia University, RT9W, Palisades, NY 10964-8000.
E-mail: visbeck@ldeo.columbia.edu

retical studies have begun to address the role of baroclinic eddies. Herman and Owens (1993) investigated the energetics of "chimney collapse" and found that small chimneys adjust and spin down primarily due to wave radiation, while chimneys of many Rossby radii in diameter break up due to baroclinic instability. Legg and Marshall (1993), using point-vortices (hetons) and laboratory experiments by Ivey et al. (1995) and Brickman (1995), found that, if buoyancy loss from the sea surface persists, the *lateral* transport of buoyancy by baroclinic eddies can completely offset this loss yielding quasi-steady chimney properties.

In this paper, we attempt to arrive at some quantitative understanding of the role of geostrophic eddies in the dynamics of isolated convective regions, their efficiency in the transport of buoyancy laterally between the chimney and the ambient ocean, and the consequences of such buoyancy transfer for the ultimate depth to which convection penetrates. In section 3 we estimate, using energetic arguments, the magnitude of the lateral buoyancy flux across a baroclinic zone due to its baroclinic instability. In section 4 the implication of such lateral fluxes for the gross behavior of the chimney is studied. In particular, we consider the maximum depth to which a chimney created by localized buoyancy loss can penetrate into a stratified fluid. We then go on to inspect laboratory and numerical experiments to gain supporting evidence, or otherwise, for the key predictions of our theory. Finally, the implications of our work for deep-water formation in the oceans are discussed.

2. Vertical mixing by convection and horizontal transfer by baroclinic eddies

Consider an ocean with uniform stratification N exposed to surface buoyancy loss B_0 over a disk of radius r, at a latitude where the Coriolis parameter is f (Fig. 1a).

Surface waters beneath the cooling disk will become dense and overturn, forming a convectively modified layer of depth h. Toward the center of the cooling disk, fluid will not be aware of the spatial inhomogeneity in the cooling—here the mixed layer will deepen, at least initially, in a one-dimensional manner. The buoyancy equation for the mixed layer is

$$\frac{Db}{Dt} = \mathbf{B}, \tag{1}$$

where $b = -g(\sigma/\rho_0)$ is the buoyancy, with σ the potential density, g the acceleration due to gravity, ρ_0 a constant reference value of density, and D/Dt the total derivative. The buoyancy forcing is $\mathbf{B} = \partial B/\partial z$, where B is the buoyancy flux. Neglecting horizontal advection and integrating (1) over the mixed layer subject to a buoyancy loss B_0 at the surface and zero buoyancy flux through its base, we obtain

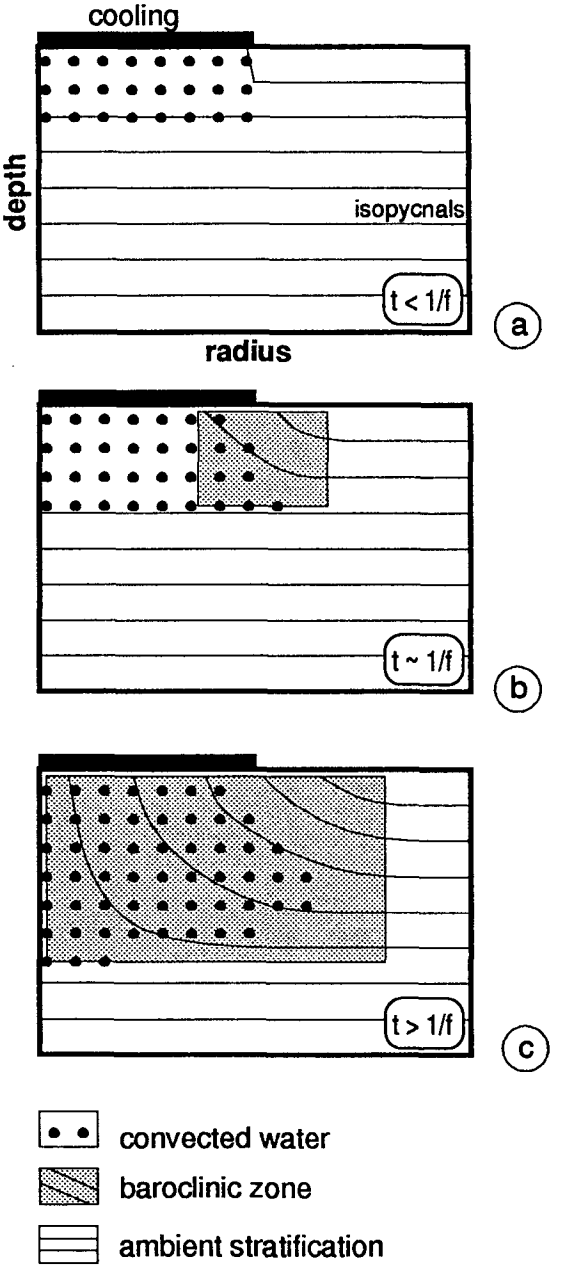

FIG. 1. Sketch of a radial cross section through a chimney characterizing three different phases of chimney development. The region of surface buoyancy loss is marked by a heavy line. The solid lines represent isopycnals. (a) Initially a convectively mixed layer is created under the cooling region. (b) As time proceeds, the edge of the convective zone adjusts under the influence of gravity and rotation to support a rim current in thermal wind balance with the baroclinic zone of Rossby radius width. (c) After some time the rim current becomes baroclinically unstable and baroclinic eddies transfer buoyancy laterally, broadening the baroclinic zone. Finally a quasi-steady state is reached in which lateral eddy transfer offsets surface buoyancy loss.

$$\frac{\partial b}{\partial t} = \frac{\partial b}{\partial z}\frac{\partial h}{\partial t} = \frac{B_0}{h}. \quad (2)$$

For a uniformly stratified fluid

$$N^2 = \frac{\partial b}{\partial z}. \quad (3)$$

Equation (2) leads to the well-known result for the nonpenetrative deepening of a mixed layer (see, for example, Turner 1973):

$$\frac{\partial h}{\partial t} = \frac{B_0}{N^2 h}, \quad \text{or} \quad h = \frac{(2B_0 t)^{1/2}}{N}. \quad (4)$$

In deriving (4) it has been assumed that (i) the overturning of the convective layer is sufficiently rapid to maintain it close to vertically mixed and (ii) buoyancy fluxes across the base of the mixed layer due to entrainment can be neglected [see Manins and Turner (1978) for a discussion]. Note that Eq. (4) is independent of rotation. Rotation can affect the buoyancy budget of a mixed layer by inhibiting vertical exchange and thereby supporting a vertically unstable density gradient layer. However, for parameters typical of ocean convection, the magnitude of this adverse gradient is orders of magnitude smaller than the ambient stratification N (see Klinger and Marshall 1995). Thus, it is a good approximation to assume that the convecting layer is well mixed. Rotation also reduces the efficiency of the turbulent entrainment process at the base of the mixed layer. Indeed, the laboratory experiments of Ivey et al. (1995) and high-resolution numerical studies of Legg et al. (1995, personal communication) all support the idea that, to a good approximation, a deep convective mixed layer deepens according to (4).

Since away from the disk of cooling the stratification takes up its ambient value, measured by N, and in the center of the chimney the stratification has been eroded away, then around the periphery of the chimney isopycnal surfaces will bow up from their resting level to cut the ocean's surface (Fig. 1b). Associated with the tilting isopycnal surfaces a thermal wind is set up within a rotational period or so establishing a "rim current" around the chimney. The width of the rim current region and its baroclinic zone will be initially of the order of the Rossby radius of deformation. Moreover, the rim current will be susceptible to baroclinic instability.

At the center of the chimney the mixed layer will deepen like $\sqrt{t}$, Eq. (4), until the growing baroclinic instability begins to sweep the water surrounding the cooling disk into the chimney and carry convected fluid outward and away below. Now the width of the baroclinic zone grows with time due to lateral buoyancy transfer by the eddies (Fig. 1c). If the cooling persists, the rate of deepening will be slowed, and may eventually be halted by finite-amplitude baroclinic eddies. This limit, in which the lateral flux balances loss from the surface, was studied in the context of a "heton" model in Legg and Marshall (1993).

The sequence of events described above and sketched in Fig. 1 can clearly be demonstrated by numerical experiment: Fig. 2 presents a simulation of the deepening of a chimney into a stratified resting fluid (in which N, measured against the Coriolis parameter f, is $N/f = 5$). Buoyancy was removed from a resting, stratified fluid over a disk 16 km in diameter at the center of the domain. The resolution of the nonhydrostatic model [the MIT model is fully described in Marshall et al. (1996, 1995, manuscript submitted to *J. Geophys. Res.*)] is ~250 m, sufficient to resolve baroclinic eddies as well as gross aspects of the convective plumes themselves. After two days convective plumes are present in the interior of the cooling region "burrowing" into the stratified fluid beneath; a rim current is beginning to develop meanders, evidence of baroclinic instability. By the end of day four, a wavenumber-five baroclinic instability is clearly visible, while upright convection has diminished in intensity. Finally, at day six, the plumes have all but disappeared and five large instability eddies are breaking the chimney apart, sweeping light fluid inward and thereby arresting the downward penetration of the mixed layer.

A different measure of the ambient stratification and hence the chimney stability is given by the Burger number

$$\mathrm{Bu} = \frac{N^2 h^2}{f^2 r^2} = \left(\frac{L_\rho}{r}\right)^2, \quad (5)$$

which compares the chimney radius to the Rossby radius of deformation. "Small" chimneys collapse due to gravity wave radiation while "large" chimneys break up due to baroclinic instability, which transfers energy more efficiently but takes longer to develop (Herman and Owens 1993; Legg and Marshall 1993). The large chimney regime is of interest here since chimneys of several Rossby radii width were observed in deep-water formation sites (MEDOC Group 1970; Leaman and Schott 1991).

The breakup of a larger chimney, 80 km in diameter, in a more strongly stratified ocean ($N/f = 18$) is shown in Fig. 3 [this calculation was carried out by A. Lascaratos (1994, personal communication) using the MIT model]. It takes much longer (~3 weeks) for the eddies to be "felt" at the center of the cooling region. In contrast to the 16-km chimney some eddies propagate out of the rim current region and establish a baroclinic zone much wider than an eddy diameter, but once again the deepening mixed layer is arrested by baroclinic eddy transfer.

These experiments vividly illustrate the two processes at work in an oceanic convective regime: upright plume convection and eddy generation due to baroclinic instability of the rim current. If the surface buoyancy loss is sustained, quasi-horizontal eddy transfer

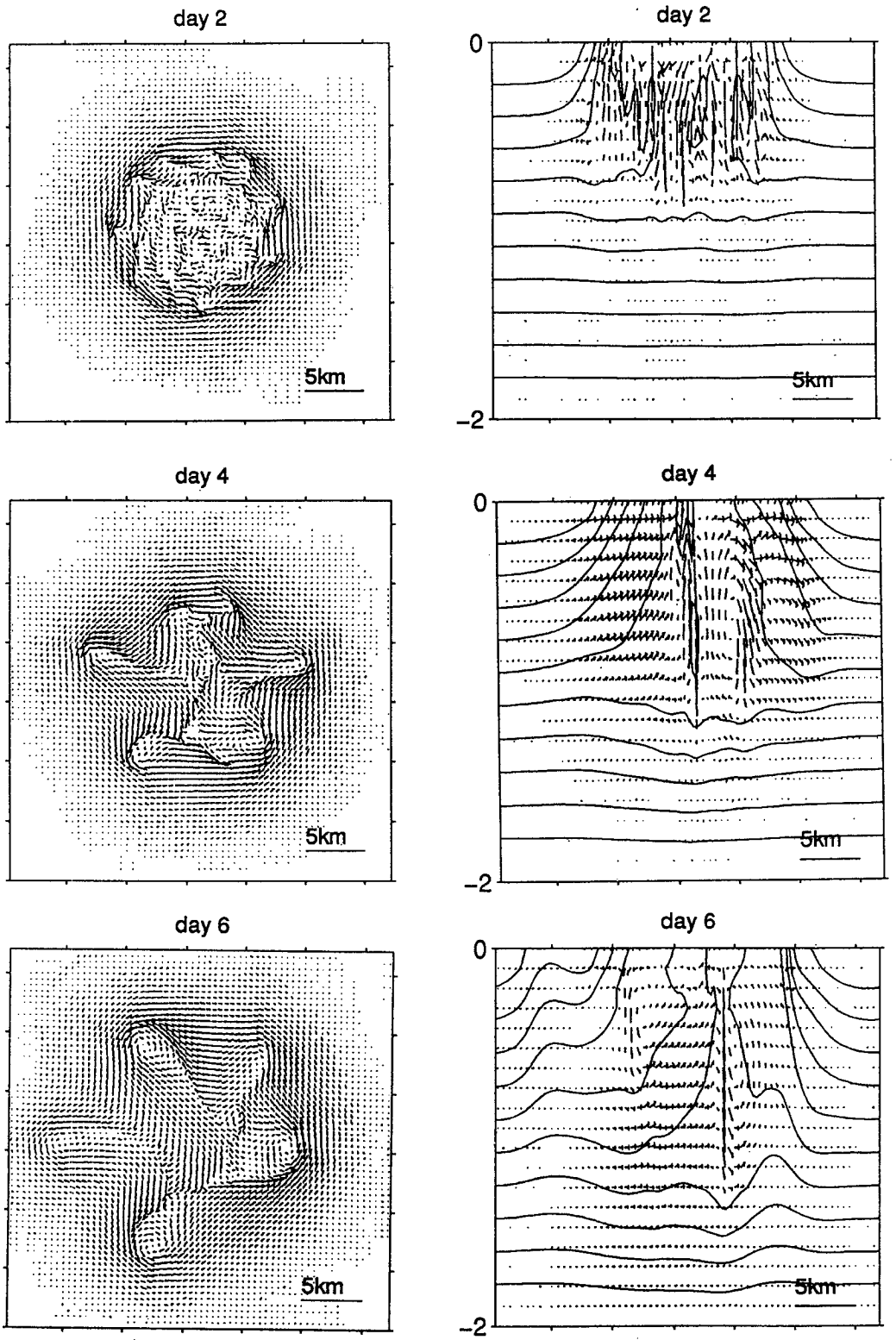

FIG. 2. Numerical simulation of a convecting chimney of radius 8 km in which convective plumes are resolved. On the left, horizontal velocity fields at a depth of 200 m are plotted; to the right, radial sections through the chimney center contouring the temperature and the velocity field in the plane of the section. The contour interval for temperature is 0.025°, and varies from 12° to 11.75° over the 2-km total depth ($N^2 = 2.5\ 10^{-7}\ s^{-2}$). Velocity vectors are plotted at every other grid point in the horizontal (horizontal resolution is 250 m), and vertical velocities have been scaled to highlight downwelling. After 2 days the maximum horizontal velocity v_{max} at 200-m depth is 16 cm s^{-1} ($w_{min} = -5$ cm s^{-1}). After 4 days, $v_{max} = 24$ cm s^{-1} ($w_{min} = -9$ cm s^{-1}), while after 6 days $v_{max} = 32$ cm s^{-1} ($w_{min} = -10$ cm s^{-1}).

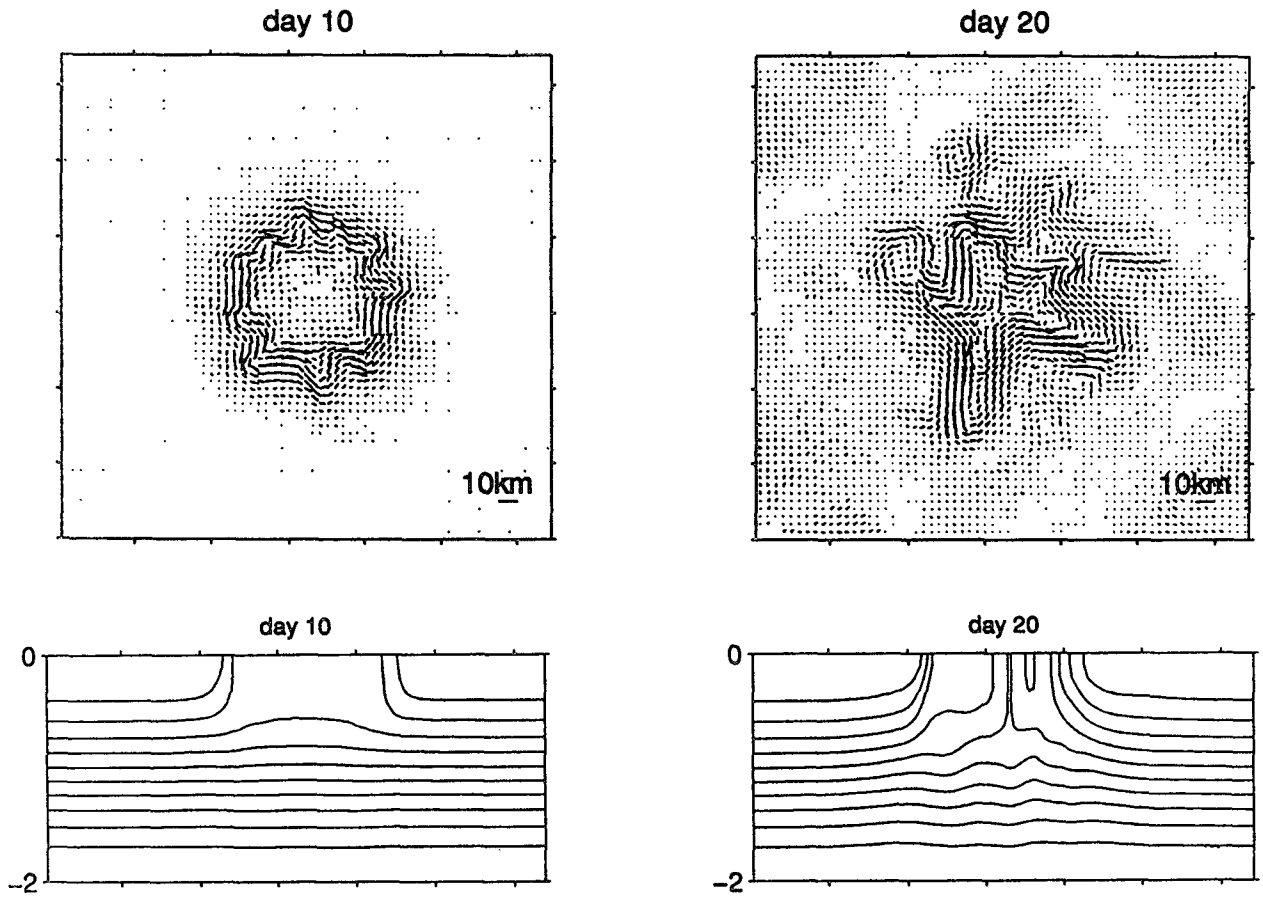

FIG. 3. Numerical simulation of a 40-km radius chimney; convection is parameterized (A. Lascaratos, 1994 personal communication). Horizontal velocity fields are shown in the upper panels. Radial sections through the center of the chimney show temperature in the lower panels. The contour interval is 0.03°; the temperature varies from 17° to 14° over the 2-km total depth ($N^2 = 3.0 \times 10^{-6}$ s^{-2}). Velocity vectors are plotted at every other grid point in the horizontal. After 10 days the maximum horizontal velocity v_{max} at 200-m depth is 24 cm s^{-1}. After 20 days, $v_{max} = 48$ cm s^{-1}. Upright convection was parameterized using the scheme of Klinger et al. (1996).

becomes increasingly important and ultimately the vertical buoyancy transfer in the eddies dominates that of the plumes. In order to quantify the effect of baroclinic eddies we now make use of "parcel theory" to estimate an upper bound on the efficiency of the baroclinic process.

3. The energetics of baroclinic waves

We briefly review the ideas explored by Green (1970) (see also Stone 1972), which led to his parameterization of the transfer of buoyancy by baroclinic instability in the atmosphere, and go on to apply them to the instability of the baroclinic zone surrounding an oceanic chimney.

Rather close analogies can be drawn between the role of geostrophic eddies in the dynamics of convective chimneys in the ocean and the role of synoptic-scale systems in the general circulation of the atmosphere. In the latter, synoptic-scale baroclinic eddies in the tropospheric jet stream transfer heat poleward and upward to balance the radiative loss of energy at upper levels over polar regions and gain in tropical latitudes. In our oceanic problem, buoyancy loss over the chimney is offset, in part, by the inward and upward flux of buoyancy due to baroclinic eddies developing in the rim current. The center of the disk in the experiment described previously can be likened to the North Pole. These eddies are entirely analogous to their atmospheric counterparts, extracting potential energy stored in the baroclinic zone where isopycnal surfaces slope upward toward the center (the pole) of the chimney (Fig. 4).

To make the connection between oceanic and meteorological contexts as explicit as possible, we adopt coordinates (y, z)—see Fig. 4—where y points radially inward (poleward) and z upward. In this coordinate frame the mean slope of isopycnal surfaces in the region of the rim current, a key quantity in the energetic analysis presented below, is positive. The

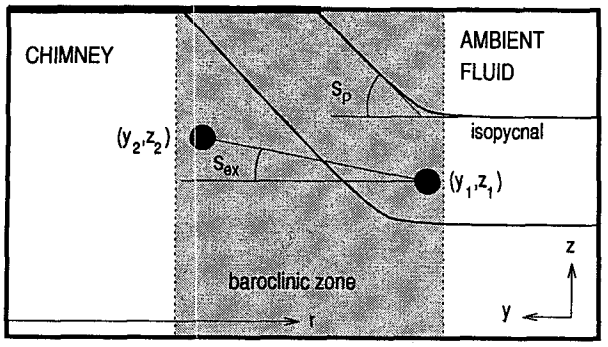

FIG. 4. Schematic vertical section through the baroclinic zone at the edge of an oceanic chimney used in applying parcel theory to enquire into the energetics of the baroclinic zone. The slope of the isopycnal surfaces is s_ρ, the slope of the surface along which parcels at (y_1, z_1), (y_2, z_2) are exchanged is s_{ex}.

slope of the isopycnals (s_ρ) within the baroclinic zone is given by

$$s_\rho = \frac{M^2}{N^2}, \tag{6}$$

where

$$M^2 = \left|\frac{\partial b}{\partial y}\right| \quad \text{and} \quad N^2 = \left|\frac{\partial b}{\partial z}\right| \tag{7}$$

are measures of the lateral and vertical "stratification" in the baroclinic zone.

Let us suppose that instability of the rim current achieves an exchange of fluid parcels between (y_1, z_1) and (y_2, z_2), as sketched in Fig. 4. The accompanying change in mean flow potential energy $\Delta\bar{P}$ is

$$\Delta\bar{P} = \rho_0 N^2 (y_2 - y_1)^2 s_{ex}(s_{ex} - s_\rho), \tag{8}$$

where $s_{ex} = (z_2 - z_1)/(y_2 - y_1)$ is the slope of the surface of exchange and the overbar indicates mean (time and azimuthally averaged) flow. The sign of $\Delta\bar{P}$ is the same as that of the factor $s_{ex}(s_{ex} - s_\rho)$ and so potential energy will be released ($\Delta\bar{P} < 0$) if the slope of the surface of exchange is *smaller* than that of the mean isopycnal surfaces ($s_{ex} < s_\rho$). The *maximum* release of energy occurs when the surface of exchange has one half of the slope of the isopycnals

$$s_{ex,max} = \frac{s_\rho}{2},$$

yielding a potential energy release of

$$|\Delta\bar{P}|_{max} = \frac{\rho_0 N^2}{4}(y_2 - y_1)^2 s_\rho^2 = \frac{\rho_0}{4}\frac{M^4}{N^2}\Delta Y^2, \tag{9}$$

where $\Delta Y = |y_2 - y_1|$ is the lateral displacement of the fluid parcels.

If all the available potential energy is converted into kinetic energy of (quasi two-dimensional) eddying motion

$$|\Delta\bar{P}|_{max} = \mathrm{KE}' = \frac{1}{2}\rho_0(u^2 + v^2) = \rho_0 V'^2,$$

an upper limit is set on a typical horizontal isotropic eddy speed V', thus

$$V'_{max} = \frac{\Delta Y}{2N} M^2 = \frac{1}{2}\frac{b'}{N}, \tag{10}$$

where

$$b' = \Delta Y M^2 \tag{11}$$

is the buoyancy anomaly of a particle displaced a distance ΔY across the zone whose lateral stratification is measured by M^2 [Eq. (7)].

We now assume that the lateral flux of buoyancy due to baroclinic eddies is given by the correlation between the eddy velocity and buoyancy anomaly, thus

$$\overline{v'b'} = \alpha\frac{\overline{b'^2}}{N}, \tag{12}$$

where (10) had been used and α is a correlation coefficient. Equation (12) can be compared to Green's (1970) Eq. (5), to which it is identical if it is remembered that his thermodynamic variable Φ is related to our buoyancy by $\Phi = -\ln\sigma = -\ln(-b\rho_0/g)$. Using atmospheric observations, Green (1970) estimated the correlation coefficient α in (12) to be 0.005 for synoptic-scale systems.

The slope of the surface of maximum energy release implies a vertical buoyancy flux

$$\overline{w'b'} = \frac{1}{2}s_\rho\overline{v'b'}. \tag{13}$$

Taken together Eqs. (11), (12), and (13) provide a "parameterization" of the lateral and vertical buoyancy flux due to baroclinic instability eddies. We now go on to investigate the implication it has for our convective scenario.

4. Baroclinic eddy transfer and the final depth scale of ocean chimneys

Let us again consider our deepening chimney, as in section 2. If the buoyancy loss is maintained for a sufficiently long period of time, the rim current around the cooling region will become baroclinically unstable and buoyancy will be fluxed by the instability eddies across the front. If the eddies are intense enough, deepening of the chimney will be arrested. In this limit, when the lateral buoyancy flux completely balances the (assumed constant) surface buoyancy loss (Fig. 5), a quasi-steady state can be established:

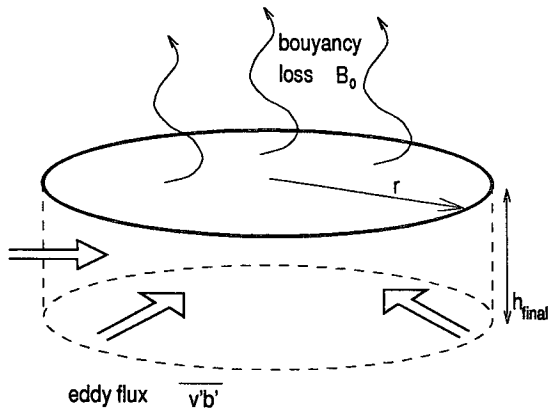

FIG. 5. A schematic diagram illustrating the balance between the surface buoyancy loss and the lateral buoyancy flux due to the baroclinic instability of an oceanic chimney.

$$\iint B_0 dA = \int_h^0 \oint \overline{v'b'} dl dz, \tag{14}$$

where the vertical integral extends from the base of the chimney to the ocean's surface and the area integral extends over the patch of buoyancy loss, assumed constant in time. Equation (14) can be used to relate $\overline{v'b'}$ to B_0: it implies that

$$\overline{v'b'} = \frac{B_0 r}{2h} = \alpha' \frac{\overline{b'^2}}{N}, \tag{15}$$

using (12), where $\overline{v'b'}$ is the lateral buoyancy flux at the radius r. Here α', which is closely related to the constant of proportionality α in (12), takes account of possible variations of the lateral buoyancy flux over the depth of the chimney.

If there is no discontinuity in density at the base of the chimney, a very reasonable assumption for a deep convective layer, then the buoyancy anomaly across the front is given by

$$b' = N^2 h. \tag{16}$$

Combining (15) with (16) we find that the deepening of the chimney is arrested at a depth given by

$$h_{\text{final}} = \gamma \frac{(B_0 r)^{1/3}}{N}, \tag{17}$$

where γ is a new constant of proportionality related to the correlation coefficient from (15) by

$$\gamma = \left(\frac{1}{2\alpha'}\right)^{1/3}. \tag{18}$$

According to (17) the final mixing depth h_{final} depends only on external parameters such as the radius of the cooling region, the strength of the cooling, and the stratification. Curiously, the final mixing depth is independent of the rate of rotation!—In the energetic arguments of section 3 leading to it, f does not directly appear. However, it is important to remember that baroclinic instability, the dynamical process that facilitates the rearrangement of fluid parcels on which the energetic argument is based, is a consequence of the thermal wind, which *is* crucially dependent on rotation.

The length scales of baroclinic eddies, assumed to be set by the Rossby radius, scale as

$$L_{\rho,\text{final}} = \frac{N h_{\text{final}}}{f} = \gamma \frac{(B_0 r)^{1/3}}{f} \tag{19}$$

and do depend on the rate of rotation f, but are independent of the ambient stratification!

At the final depth we find

$$\left.\begin{aligned} b_{\text{final}} &= N^2 h_{\text{final}} = \gamma N (B_0 r)^{1/3} \\ V_{\text{eddy,final}} &= \frac{b_{\text{final}}}{2N} = \frac{\gamma}{2} (B_0 r)^{1/3} \end{aligned}\right\} \tag{20}$$

—all independent of rotation. It is reassuring to note that the quantities $L_{\rho,\text{final}}$, $V_{\text{eddy,final}}$, and b_{final} are in thermal wind balance with one another.

a. *Equilibrium timescale*

Can we estimate how long it takes to reach this quasi-equilibrium state? It must take at least the time required by one-dimensional mixing to reach the depth h_{final}: from (4) and (17) we deduce that

$$t_{\text{final}} \geqslant \frac{\gamma^2}{2} \left(\frac{r^2}{B_0}\right)^{1/3}. \tag{21}$$

Consistently, the final timescale is independent of the rate of rotation, increases with the radius of the cooling region r, and decreases with the surface buoyancy flux B_0. Equation (21) suggests then, that

$$t_{\text{final}} = \beta \left(\frac{r^2}{B_0}\right)^{1/3}, \tag{22}$$

where β will be determined by laboratory and numerical experiments.

b. *Nondimensional parameters*

We can readily identify the controling nondimensional parameter of our problem. Dividing the final mixing depth h_{final}, Eq. (17), by the cooling radius yields the chimney aspect ratio

$$\frac{h_{\text{final}}}{r} = \gamma \left(\frac{f}{N}\right) \left(\frac{l_{\text{rot}}}{r}\right)^{2/3}. \tag{23}$$

Two nondimensional numbers appear: f/N and l_{rot}/r, where

$$l_{\text{rot}} = \left(\frac{B_0}{f^3}\right)^{1/2} \tag{24}$$

is the length scale central to the unstratified convection problem (Jones and Marshall 1993; Maxworthy and Narimousa 1994). For conditions typical of deep convection $l_{\rm rot} \sim 300$ m and $r \sim 20$ km.

The nondimensional parameter N/f sets the aspect ratio of the instability eddies, as given by (17) and (19):

$$\frac{L_{\rho,\rm final}}{h_{\rm final}} = \frac{N}{f}. \tag{25}$$

The ratio $r/l_{\rm rot}$ controls two other chimney properties of interest: the breakup timescale of the chimney and the number of eddies that form around the periphery of the chimney.

The ratio of the breakup timescale to a pendulum day ($t_{\rm rot} = 2\pi f^{-1}$) is given by

$$\frac{t_{\rm final}}{t_{\rm rot}} = \frac{\beta}{2\pi}\frac{r^{2/3}f}{B_0^{1/3}} = \frac{\beta}{2\pi}\left(\frac{r}{l_{\rm rot}}\right)^{2/3}. \tag{26}$$

The ratio between the rim current length ($2\pi r$) and the hypothesized eddy diameter ($2L_\rho$) yields

$$\frac{2\pi r}{2L_{\rho,\rm final}} = \frac{\pi}{\gamma}\frac{r^{2/3}f}{B_0^{1/3}} = \frac{\pi}{\gamma}\left(\frac{r}{l_{\rm rot}}\right)^{2/3}. \tag{27}$$

This is the expected number of eddies around the rim current in the steady state (the mode number). Finally, $r/l_{\rm rot}$ is related to the Burger number, thus

$$\mathrm{Bu}_{\rm final} = \left(\frac{L_{\rho,\rm final}}{r}\right)^2 = \gamma^2\left(\frac{l_{\rm rot}}{r}\right)^{4/3}. \tag{28}$$

In the scenario considered here, the stratification is assumed to be strong enough that the chimney is not aware of the finite depth of the ocean (but see section 6). Thus, the only externally imposed length scales are r and $l_{\rm rot}$. However, it is useful to measure them against the total water depth as follows:

$$\frac{l_{\rm rot}}{r} = \frac{H}{r}\frac{l_{\rm rot}}{H} = \delta \mathrm{Ro}^*,$$

where $\delta = H/r$ is the aspect ratio of the forcing region and

$$\mathrm{Ro}^* = \frac{B_0^{1/2}}{Hf^{3/2}} = \frac{l_{\rm rot}}{H}$$

is the convective or "natural" Rossby number, the parameter central to the unstratified convection problem studied in Jones and Marshall (1993) and Maxworthy and Narimousa (1994). The physical significance of R_0^* is discussed at some length in Marshall et al. (1994).

We now seek support for these predictions in laboratory and numerical studies of a convective chimney; implications for the ocean are postponed to the discussion.

5. Support from laboratory and numerical experiments

Various laboratory and numerical experiments (both carried out locally at MIT and Woods Hole, and elsewhere) were inspected to gain support (or otherwise) for the dependence of $h_{\rm final}$ on the external parameters as derived above and to determine the constants of proportionality γ and β. This in turn leads to an experimental determination of the correlation coefficient α' of the eddy velocity and buoyancy anomaly, Eq. (18), critical to setting the magnitude of the lateral buoyancy flux of baroclinic eddies.

A feature common to all the experiments against which our theory was tested was that a constant surface buoyancy loss was applied to a stratified fluid over a circular subdomain. The initial stratification was constant and, in most cases, strong enough to prohibit convection through the whole depth of the column.

Our numerical experiments used the nonhydrostatic model described in Marshall et al. (1996, manuscript submitted to *J. Geophys. Res.*, 1995) with a horizontal resolution of 250 m and a vertical grid spacing of 100 m. Some calculations employed a larger horizontal grid spacing of 2 km, which could not resolve the plumes. In these experiments a vertical adjustment scheme was implemented (Klinger et al. 1996) to parametrically represent the effect of mixing by plumes.

In addition, data from two independent series of laboratory experiments were analyzed. In one laboratory setup a hot plate introduced buoyancy into a thermally stratified ocean from below (Ivey et al. 1995). In the other series, described in Whitehead et al. (1996, manuscript submitted to *J. Geophys. Res.*), salty water was sprayed over a circular region at the surface of a haline-stratified fluid.

The external parameters of all experiments were the surface buoyancy flux B_0 applied over a disc of radius r, the stratification N of the ambient fluid, and the rate of rotation f. As we shall see, taken together these experiments cover a fairly wide range of the relevant nondimensional parameters, and span the regime of interest for the ocean.

Each experiment was analyzed to determine the "quasi-final" mixing depth of the chimney. A number of different criteria were used: a water-mass census, a time series of surface density or inspection of pictures, and plots of vertical model sections. Details of our analysis procedures are given in the appendix.

For example, the evolution of the surface density, averaged over a 2.5-km diameter circular region centered on the cooling disc of the numerical experiment shown in Fig. 2, is plotted in Fig. 6. Initially the density anomaly is well tracked by the one-dimensional mixed layer prediction, Eqs. (4) and (16). However, as time progresses, the data "roll off" the $t^{1/2}$ curve as eddies sweep buoyant water in from the side. The depth of the chimney inferred from the surface density anomaly

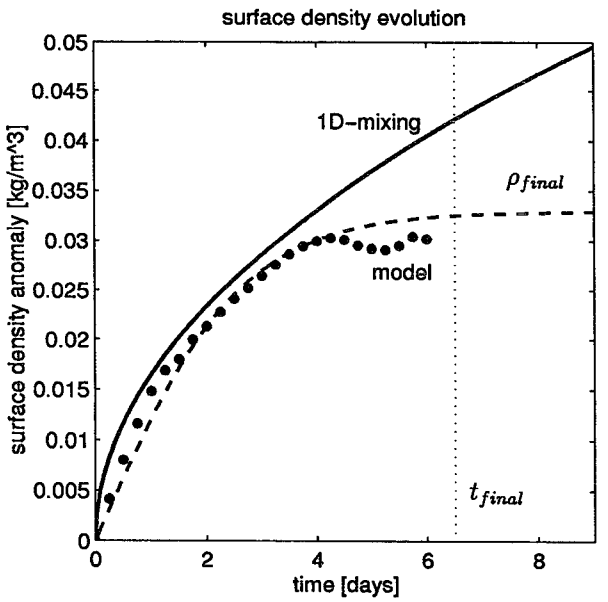

FIG. 6. Evolution of the surface density in a convecting chimney. The solid line indicates the density evolution predicted by one-dimensional mixing theory, Eq. (4). The dots represent the surface density of a numerical chimney simulation averaged over a 2.5-km radius. The externally imposed parameters were $B_0 = 3.9 \times 10^{-7}$ $m^2 s^{-3}$, $N^2 = 4 \times 10^{-7}$ s^{-2}, $f = 10^{-4}$ s^{-1}, and $r = 8000$ m. The dashed line is given by

$$\rho'(t) = \gamma \frac{\rho_0 N}{g} (B_0 r)^{1/3} \tanh\left(\frac{2.5}{\beta} \frac{B_0^{1/3}}{r^{2/3}} t\right),$$

where ($\gamma = 3.5$ and $\beta = 10$). It asymptotes to ρ'_{final} at a time t_{final}.

clearly shows that the deepening of the chimney is arrested.

Figure 7 plots the diagnosed final mixing depth of all experiments versus the predicted h_{final}, both normalized by the size of the forcing region r. The mean constant of proportionality in (17) was found to be

$$h_{\text{final}} = \gamma \frac{(B_0 r)^{1/3}}{N}; \quad \gamma = 3.9 \pm 0.9, \qquad (29)$$

where the error bars represent the standard deviation of all experiments. In Fig. 8 the observed final mixing depth, normalized by the prediction $h_{\text{final}} = (B_0 r)^{1/3} N^{-1}$, is plotted against N/f and r/l_{rot}, the two nondimensional parameters central to this problem (see previous section). Although there is overall agreement, Fig. (8a) suggests a possible trend toward a larger than expected final mixing depth with increasing stratification. However, plotting $h_{\text{obs}}/h_{\text{final}}$ versus r/l_{rot} shows that most of the scatter occurs for small chimneys (small r/l_{rot}, large Burger number). Our theory, however, assumes a small Burger number (5); reassuringly data from those experiments with large r/l_{rot} ratios collapse onto the line more than data from experiments with small r/l_{rot} (Fig. 8b). For these large chimney experiments it seems that the depth to which the chimney penetrated is indeed independent of rotation, as expected from (17).

In Fig. 9 we plot the time (normalized by the rate of rotation f) taken to reach the quasi-equilibrium state versus the prediction $t_{\text{final}} \sim r^{2/3}/B_0^{1/3}$. The small tank experiments by Whitehead et al. (1996, manuscript submitted to *J. Geophys. Res.*) could not be fully analyzed for their temporal evolution, but the other sets of experiments yielded a constant of proportionality of

$$t_{\text{final}} = \beta \frac{r^{(2/3)}}{B_0^{(1/3)}}; \quad \beta = 12 \pm 3, \qquad (30)$$

where the error represents the standard deviation of all experiments. It is reassuring that β is somewhat larger than (about twice) the lower limit predicted by (22) and (29), which is $\gamma^2/2 = 6.5$.

Using (18) we can relate the value of γ to the correlation of the eddy velocity and the buoyancy anomaly. We find α' from (18) and (29) to be

$$\alpha' = \frac{1}{2\gamma^3} = 0.008 \pm 0.005, \qquad (31)$$

which is remarkably close to the atmospheric value deduced by Green (1970) of 0.005.

Range of nondimensional parameters

In the experiments considered here the nondimensional parameters N/f and r/l_{rot} ranged through roughly two orders of magnitude as can be seen in Fig. 10. We

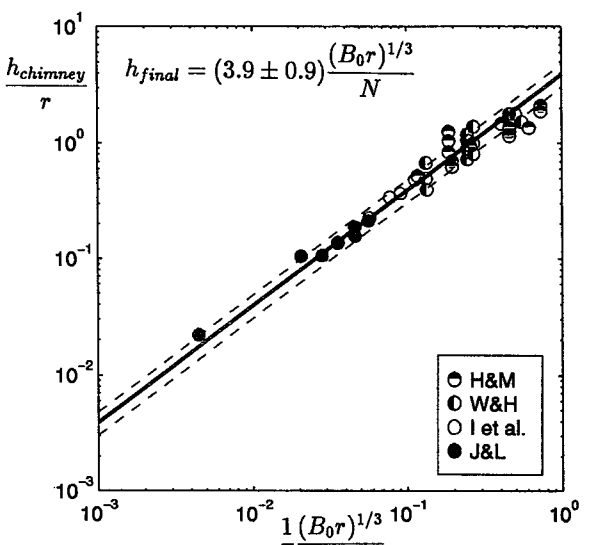

FIG. 7. Regression of the final observed chimney depth versus the prediction $h_{\text{final}} = (B_0 r)^{1/3}/N$ both normalized by the radius of the surface cooling r. H&M indicate numerical simulations from Hufford and Marshall, W&H indicate laboratory experiments from Hufford and Whitehead, I et al. refer to the laboratory work from Ivey et al., and J&L represent numerical simulations by Jones and Lascaratos.

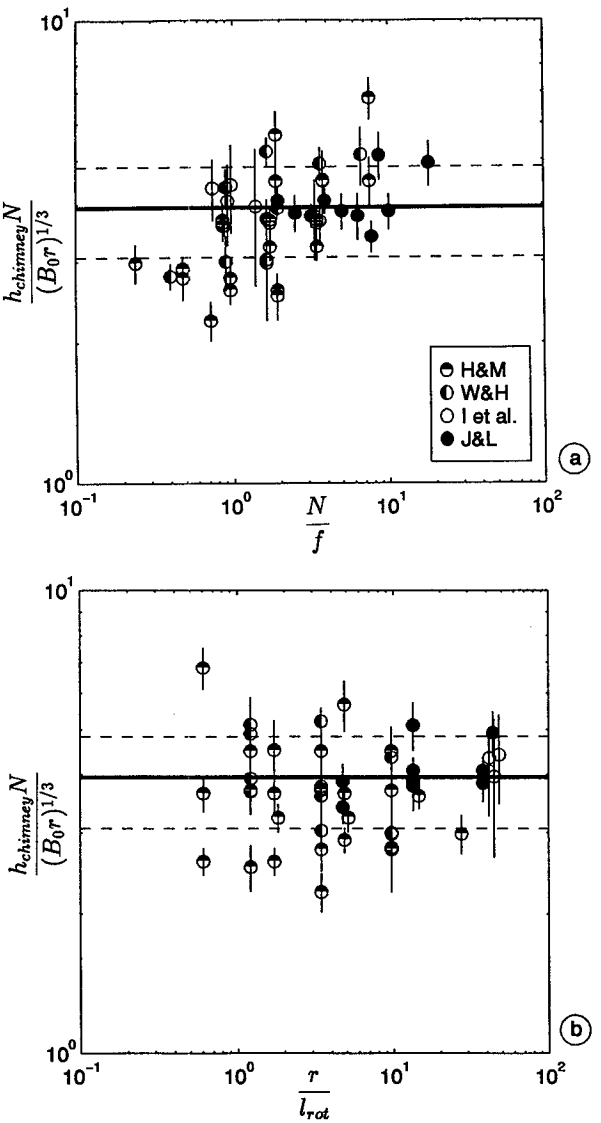

FIG. 8. Scatterplot of the parameter $\gamma = h_{\text{final,observed}}/h_{\text{final,theory}}$ versus (a) N/f and (b) r/l_{rot}. Error bars and regression lines are included.

have included additional vertical axes to indicate the final mode number of instability (27) and the number of pendulum days required to reach the steady state (26). Further, it seemed useful to us to also include in Fig. 10 lines of constant chimney aspect ratio (23), which then allows one to find the final mixing depth graphically. For example, returning to the numerical calculation depicted in Fig. 2, for which $N/f = 5$ and $r/l_{\text{rot}} = 12$, Fig. 10 yields a chimney aspect ratio of $r/h_{\text{final}} = 8$ with a final mixing depth of ~1000 m, a mode number of 5, and a time for the chimney to reach its equilibrium depth of 8 pendulum days.

Overall, there is encouraging agreement between the disparate experiments reviewed here, both laboratory and numerical, and the proposed scaling. If the buoyancy forcing persists for a long enough period, a quasi-steady state will be reached, limiting the depth of the chimney and setting an upper limit on the density gradient across the rim current. Moreover, the experiments provide quantitative support for Green's energy arguments that were used to quantify the lateral flux of buoyancy due to baroclinic eddies.

6. Chimney dynamics in neutral and weakly stratified oceans: the effect of the bottom

If care is taken, the arguments presented in sections 3 and 4 can also be applied to an ocean that is initially weakly stratified or even unstratified, the focus of a number of laboratory (Maxworthy and Narimousa 1994; Brickman 1995) and numerical experiments (Jones and Marshall 1993; Send and Marshall 1995). In this parameter regime the total water depth H is shallower than the final mixing depth

$$\frac{h_{\text{final}}}{H} = \gamma \frac{(B_0 r)^{1/3}}{NH} > 1. \tag{32}$$

In other words, if the initial stratification is weaker than a critical stratification ($N < N_{\text{crit}}$) given by

$$N_{\text{crit}} = \gamma \frac{(B_0 r)^{1/3}}{H}, \tag{33}$$

then the chimney will reach to the bottom. Now baroclinic eddies will set up a stratification N_{final} within the baroclinic zone that is stronger than the initial stratifi-

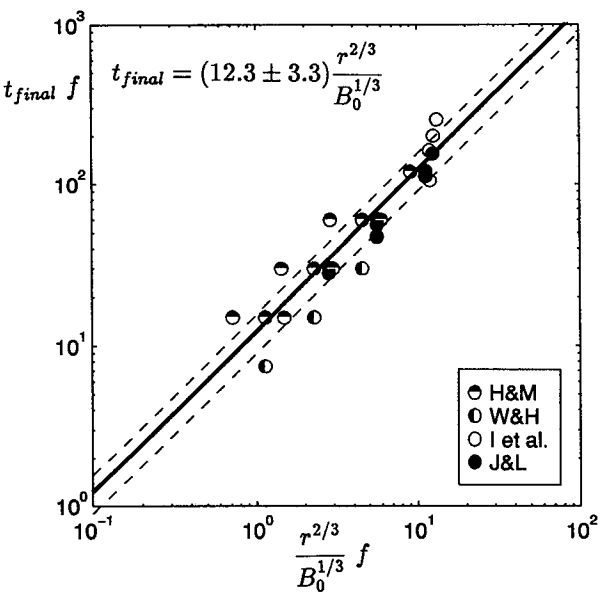

FIG. 9. Regression of the observed final timescale versus the prediction $t_{\text{final}} = r^{2/3}/B_0^{1/3}$, both normalized by the rate of rotation f. Note only the I et al. and J&L runs were used for the regression.

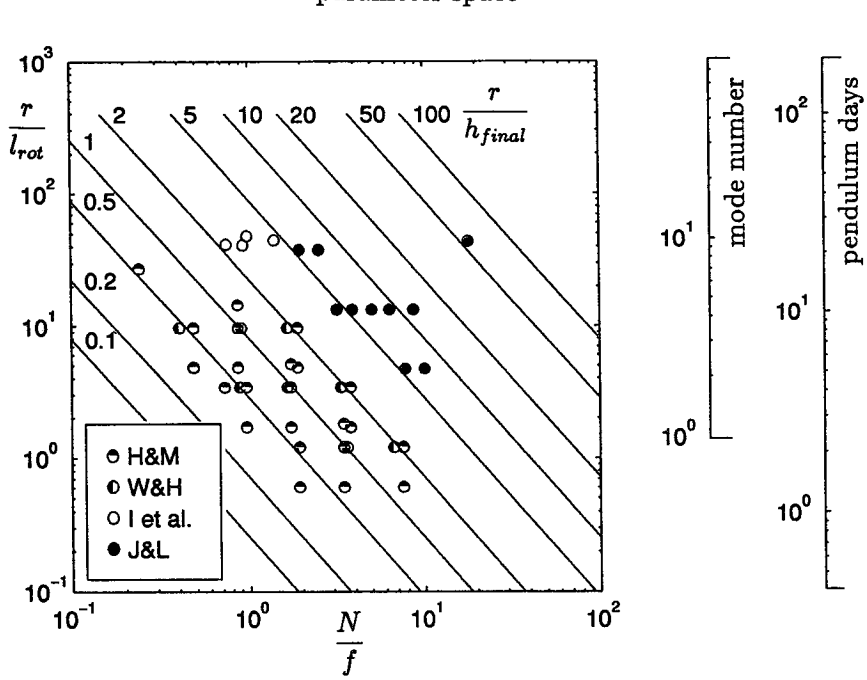

FIG. 10. The parameter space covered by all chimney experiments, both laboratory and numerical. Solid slanting lines represent constant chimney aspect ratios r/h_{final} [Eq. (23)]. Axes representing the final mode number of baroclinic instability and the predicted time (in pendulum days) to reach the steady state are also included. Axes and lines are enumerated making use of our best estimate of the constants of proportionality $\gamma = 3.9$, $\beta = 12$ deduced from Figs. 8 and 9.

cation N. Equations (15), (16) with $h = H$ implies that the buoyancy anomaly associated with the final stratification scales as

$$b_{b,\text{final}} = \gamma^2 \frac{(B_0 r)^{2/3}}{H}, \tag{34}$$

where the subscript b refers to the effect of the bottom. Making use of (16) again yields N_{final} within the baroclinic zone:

$$N_{\text{final}} = \gamma \frac{(B_0 r)^{1/3}}{H}. \tag{35}$$

Here γ is taken to be the same constant of proportionality as determined previously, 3.9 as in Eq. (29). The velocity scale $V_{\text{eddy,final}}$ and eddy size $L_{\rho,\text{final}}$ are again given by (20) and the thermal wind relation remains valid. Combining the one-dimensional buoyancy budget (2),

$$b_b(t) = \frac{B_0 t}{H},$$

with (34) allows one to estimate a lower limit on the time it takes to reach the final density:

$$t_{b,\text{final}} \geq \gamma^2 \frac{r^{2/3}}{B_0^{1/3}}, \tag{36}$$

which is identical to the stratified case (22). We now see that the weakly or unstratified case can conveniently be accommodated within the scalings derived for the stratified regime. This enables one to use Fig. 10 as a diagnostic for the weakly stratified regime also. Now the chimney aspect ratio is set by the external parameter ($r/h_{\text{final}} = r/H$), and the eddy aspect ratio ($N/f = N_{\text{final}}/f$) is the graphical solution of (35).

An interesting series of laboratory experiments in the unstratified regime was carried out by Brickman (1995), who heated fluid over a disc from below. Although the heating was constantly applied, the temperature in the chimney above it reached a quasi-constant value. Using dimensional arguments Brickman derives scaling laws for the breakup timescale ($\tau f = 4.3\ \text{Ro}^{*-2/3}$) and the final buoyancy anomaly ($b = 4.7 B_0^{2/3} H^{-1/3}$). He noted that steady-state properties were independent of rotation in agreement with our predictions [(34), (36)]. However, his scaling laws did not consider the radius of the heating disc. Multiplying Brickman's breakup timescale by $(r/H)^{2/3}$ yields our results (30) but with a constant of proportionality of 6 rather than the 12 found here. The difference of a factor of 2 can, perhaps, be attributed to the use by Brickman of a tanh function to fit the temperature evolution observed in his experiment. Here we have adopted a different measure of timescale—the time to arrive at the final quasi-steady

state—as indicated in Fig. 6. Our timescale is about twice as long as that given by Brickman's definition [note that $\tanh(1) = 0.76$, while twice the time, $\tanh(2) = 0.96 = 1 - 4\%$, close to our definition]. His estimate of the final temperature anomaly [when multiplied by $(r/H)^{2/3}$] is consistent with our result (34) but with a γ of 7.5, which is larger than our 3.9 (29). In conclusion, the scalings presented here are broadly consistent with Brickman's findings, if one takes into account the variable sizes of the forcing region and the different measures of timescale adopted.

7. Discussion

We have studied the energetics of baroclinic eddies in an idealized isolated convective regime (chimney). Lateral buoyancy fluxes due to such baroclinic eddies developing in the rim current region can ultimately offset the surface buoyancy loss and thereby arrest the deepening of the chimney. We have envisioned chimneys that are many Rossby radii wide, and therefore geostrophic adjustment and frictional spin down processes are dominated by baroclinic eddy transfer. In a strongly stratified ocean, a quasi-steady mixing depth is set up given by

$$h_{\text{final}} = 3.9 \frac{(B_0 r)^{1/3}}{N}$$

and the time it takes to the reach that final mixing depth is given by

$$t_{\text{final}} = 12 \frac{r^{2/3}}{B_0^{1/3}}.$$

What are the implications of these results for deep-water formation in the ocean? First, consider the northwestern Mediterranean MEDOC region. In bottom-water formation found in 1987 (Schott and Leaman 1991; Leaman and Schott 1991) the observed chimney, though not strictly circular, had a width of at least 60 km. A typical mistral heat loss (600 W m^{-2}) yields $(r/l_{\text{rot}}) \sim 100$ and, since convection reached to the bottom (2000 m) during that year, the chimney aspect ratio was $(r/H) \sim 15$. Inspection of Fig. 10 then yields an equilibrium stratification $(N_{\text{final}}/f) \sim 2.5$ for the rim current region. Observations typically show a top to bottom density difference of 0.02 kg m^{-3}, yielding $N \sim 3 \times 10^{-4}$ s^{-1} in broad agreement with our scaling.

In the winter of 1969 (MEDOC Group 1970) and 1992 (THETIS Group 1994) convection did not reach the bottom but stopped at intermediate levels. Perhaps deepening of the chimney was arrested due to lateral eddy-induced buoyancy flux offsetting the surface cooling. Our findings suggest that for a Mediterranean chimney, $t_{\text{final}} = 12 r^{2/3} B_0^{-1/3} \sim 30$ days, inserting typical values above. Therefore, it seems unlikely that baroclinic eddies played a central role in arresting the deepening chimney because the period of strong heat loss lasted only 10 days. However, close to the rim current significant lateral heat and tracer fluxes must have occurred, associated with geostrophic eddies. Our prediction for a typical eddy size, given by the final Rossby radius, is close to the observations; Eq. (19) suggests a Rossby radius of 8 km, which is roughly in accord with the eddy scales observed by Gascard (1978).

Baroclinic eddy fluxes are likely to be of great importance, however, on the seasonal timescale because the geostrophic eddy instability time is then considerably shorter than that of the forcing. If the heat loss is ~200 W m^{-2} and the diameter of the convecting region ~200 km, parameter perhaps more typical of the Labrador Sea gyre, then (30) yields a breakup timescale of ~60 days. This suggests that by the end of winter baroclinic eddies can influence the mixed layer budget significantly, even at the center of the gyre.

Where are the limitations of our findings? Throughout the study we have assumed that upright plume convection can be represented by rapid vertical mixing. In particular, we have made use of Eq. (4), which assumes a fast and efficient vertical mixing process accompanied by only small turbulent mixing at the base of the mixed layer (the nonpenetrative convection limit, Manins and Turner 1978). We have further assumed that the frictional spindown of a geostrophically balanced chimney is weaker than the anticipated transfer due to baroclinic eddies. As shown by Herman and Owens (1993), this is true for chimneys much larger than the radius of deformation. Some of the laboratory experiments of (Whitehead et al. 1996, manuscript submitted to *J. Geophys. Res.*), however, were in a Burger number regime of $O(1)$ and showed somewhat shallower final mixing depths than predicted. Moreover, there is a richness of behavior evident in the experiments: Medium size chimneys collapsed by the growth and decay of rim current meanders, while large chimneys seemed to shed eddies out of the rim current region reminiscent of the heton experiments of Legg and Marshall (1993). We suspect that the final Burger number [$\text{Bu}_{\text{final}} \sim (l_{\text{rot}}/r)^{4/3}$] can be used to distinguish between a meandering and a hetonic regime.

It is noteworthy that the efficiency with which baroclinic eddies transform available potential energy into eddy kinetic energy yields a lateral buoyancy flux in our chimney that scales similarly to that of their atmospheric counterparts. The parameter α in Eqs. (12), (15) is $\alpha_{\text{ocean}} = 0.008$ in our oceanic chimney and $\alpha_{\text{atmos}} = 0.005$ in the atmosphere (Green 1970). Stone (1972) derived a somewhat similar eddy transfer scheme using linear theory and showed that it agrees with Green's version if α scales as the Burger number [Stone's Eq. (2.30)]:

$$\alpha_{\text{Stone}} = 0.2\ \text{Bu} = 0.2\left(\frac{L_\rho}{L}\right)^2,$$

where L_ρ denotes the Rossby radius and L is the width of the baroclinic zone. In the atmosphere Stone's prediction of α agrees with the observations if Bu = 0.03, implying a ratio of $L/L_\rho = 6$, much as is observed. In the chimney experiments, however, the Burger number varied considerably from about 6 to 0.07; if we assume that α depends on the Burger number in the manner suggested by Stone, then we find less agreement between the predicted and modeled final chimney depths.

In conclusion, parcel theory was used to estimate the lateral buoyancy flux due to baroclinic eddies and yielded scaling laws that account for many of the gross chimney properties observed in diverse numerical and laboratory models. This suggests that such ideas may provide a useful starting point from which to begin developing parametric representations of geostrophic eddy transfer for the use in coarse-resolution models that do not explicitly represent them. Such developments will be reported in a later paper.

Acknowledgments. We would like to thank G. Hufford, A. Lascaratos, and J. Whitehead for letting us inspect their laboratory and numerical model simulations. B. Klinger, S. Legg, J. Marotzke, D. Marshall, and P. Stone contributed by helpful discussions. MV was funded by a UCAR/NOAA postdoctoral fellowship on Global and Climate Change. JM received support from the Atlantic Climate Change Program of NOAA and the Office of Naval Research. HJ was supported by the MAST II program of the EEC as part of MERMAIDS.

APPENDIX

Evaluation of Mixing Depths in Laboratory and Numerical Models

To obtain the final mixing depth of the quasi-steady state in various laboratory and numerical experiments a number of criteria were used. Here we briefly review the procedures used and explain the expected errors.

a. Laboratory results from Ivey et al. (1995)

Ivey and collaborators were concerned with convective mixed layer growth in a rotating stratified fluid. In a number of their experiments the mixed layer penetration was arrested before reaching the weakly stratified layer. We have made use of four such runs: experiments: 7, 8, 22, and 31. Ivey et al. determined the mixed layer depth by inspecting thermistor data from the center of the chimney. The final depth and timescale used here was estimated from their Fig. 9 and an error estimated from the scatter of the points in that figure.

b. Laboratory and numerical results from Whitehead et al.

The mixing depth was evaluated in the laboratory by observing the penetration of the dyed salt solution used to induce convective deepening. These measurements were taken by eye and an uncertainty of ± 1.5 cm was reported. It was difficult to measure the time it took for the chimney to reach a steady state and the estimates were therefore not included in the regression (Fig. 9).

Some of the laboratory experiments were also simulated on a computer using the MIT ocean model. The depth to which convection penetrated was deduced by inspecting a water mass census at several times during the integration. A peak in a salinity histogram indicated that this water mass was formed by convection. The peak salinity was then converted to a depth by making use of the initial salinity profile. We have adopted an uncertainty of ± 2 cm to the depths deduced by this histogram method.

c. Further numerical experiments

We performed a series of experiments enquiring into the dynamics of convective chimneys using the MIT model. For these experiments many "snapshots" were available and allowed a careful inspection of time and depth scales. Initially the mixing depth was inspected by eye from figures similar to Fig. 2. These estimates turned out to be as good as more elaborate methods. For example, we have averaged the temperature over the upper 300 m of the model over a disc $1/3$ of the diameter of the cooling patch to obtain the evolution of the chimney density as shown in Fig. 6 and deduced the final depth from the reference stratification. Both estimates were found to be robust and in agreement with one another; we have assumed an error for the final depth of the order of the vertical resolution (100 m) of the model. It is noteworthy that the integrations were carried out for a longer time than analyzed here. However, use of periodic boundary conditions allows eddies to reenter the domain. We therefore restricted the analysis to the first six days when not much activity occurred close to the boundaries. A recent integration in a much larger domain indicates that the results from experiments analyzed here are unchanged.

A. Lascaratos (of the University of Athens) carried out a simulation of a much larger chimney using the same model but with coarser horizontal resolution (2 km). Here convection was not resolved but represented by a large vertical diffusion. Again, the mixing depth was inspected by eye from horizontal cross sections through the chimney center and a depth error of 100 m was assumed.

REFERENCES

Brickman, D., 1995: Heat flux partitioning in open-ocean convection. *J. Phys. Oceanogr.*, **25,** 2609–2623.

Gascard, J. C., 1978: Mediterranean deep water formation, baroclinic instabilities and oceanic eddies. *Oceanol. Acta,* **1,** 315–330.

——, and A. R. Clarke, 1983: The formation of Labrador Sea Water. Part II: Mesoscale and smaller scale processes. *J. Phys. Oceanogr.,* **13,** 1779–1797.

Green, J. S. A., 1970: Transfer properties of the large-scale eddies and the general circulation of the atmosphere. *Quart. J. Roy. Meteor. Soc.,* **96,** 157–185.

Herman, A., and B. Owens, 1993: Energetics of gravitational adjustment for mesoscale chimneys. *J. Phys. Oceanogr.,* **23,** 346–371.

Hufford, G., J. Marshall, and J. A. Whitehead, 1995: Localized convection in rotating stratified fluid. *J. Geophys. Res.,* submitted.

Ivey, G., J. Taylor, and M. Coates, 1995: Convectively driven mixed layer growth in a rotating, stratified fluid. *Deep-Sea Res.,* **95,** 331–349.

Jones, H., and J. Marshall, 1993: Convection with rotation in a neutral ocean: A study of open-ocean deep convection. *J. Phys. Oceanogr.,* **23,** 1009–1039.

Klinger, B., and J. Marshall, 1995: Regimes and scaling laws for rotating deep convection in the ocean. *Dyn. Atmos. Oceans,* **21,** 227–256.

——, ——, and U. Send, 1996: Representation and parameterization of deep convective plumes by mixing. *J. Geophys. Res.,* in press.

Leaman, K., and F. Schott, 1991: Hydrographic structure of the convection regime in the Gulf of Lions: Winter 1987. *J. Phys. Oceanogr.,* **21,** 573–596.

Legg, S., and J. Marshall, 1993: A heton model of the spreading phase of open-ocean deep convection. *J. Phys. Oceanogr.,* **23,** 1040–1056.

Manins, P. C., and J. S. Turner, 1978: The relation between the flux ratio and energy ratio in convectively mixed layers. *Quart. J. Roy. Meteor. Soc.,* **104,** 39–44.

Marshall, J., J. A. Whitehead, and T. Yates, 1994: Laboratory and numerical experiments in ocean convection. *Ocean Processes in Climate Dynamics: Global and Mediterranean Examples,* P. Malanotte-Rizzoli and A. R. Robinson, Eds., Kluwer, 173–201.

——, A. Adcroft, C. Hill, L. Perelman, and C. Heisey, 1995: A finite volume, incompressible Navier–Stokes model for studies of the ocean on parallel computers. *J. Geophys. Res.,* submitted.

——, C. Hill, L. Perelman, and A. Adcroft, 1996: Hydrostatic, quasi-hydrostatic and non-hydrostatic ocean modeling. *J. Geophys. Res.,* in press.

Maxworthy, T., and S. Narimousa, 1994: Unsteady, turbulent convection into a homogeneous, rotating fluid, with oceanographic applications. *J. Phys. Oceanogr.,* **24,** 865–887.

MEDOC Group, 1970: Observation of formation of deep water in the Mediterranean Sea. *Nature,* **227,** 1037–1040.

Schott, F., and K. Leaman, 1991: Observations with moored acoustic Doppler current profilers in the convection regime in the Golfe du Lion. *J. Phys. Oceanogr.,* **21,** 558–574.

——, M. Visbeck, and J. Fischer, 1993: Observations of vertical currents and convection in the central Greenland Sea during the winter of 1988/89. *J. Geophys. Res.,* **98,** 14 401–14 421.

——, ——, and U. Send, 1994: Open ocean deep convection, Mediterranean and Greenland Seas. *Ocean Processes in Climate Dynamics: Global and Mediterranean Examples.* P. Malanotte-Rizzoli and A. R. Robinson, Eds., Kluwer, 203–225.

Send, U., and J. Marshall, 1995: Integral effects of deep convection. *J. Phys. Oceanogr.,* **25,** 855–872.

Stone, P., 1972: A simplified radiative-dynamical model for the static stability of rotating atmospheres. *J. Atmos. Sci.,* **29,** 405–418.

THETIS Group, 1994: Open-ocean deep convection explored in the Mediterranean. *Eos Trans. Amer. Geophys. Union,* **75,** 217–221.

Visbeck, M., 1993: *Konvektion im offenen Ozean. Interpretation von Beobachtungen aus der Grönlandsee und dem westlichen Mittelmeer.* Rep. 237. Institute fur Meereskunde, Kiel, Germany, 187 pp.